CrystEngComm

PAPER

Supercritical synthesis in combination with a spray process for 3D porous microsphere lithium iron phosphate†

Cite this: DOI: 10.1039/c3ce42264j

Jae-Kwang Kim[ab]

Received 6th November 2013,
Accepted 15th January 2014

DOI: 10.1039/c3ce42264j

www.rsc.org/crystengcomm

A short synthesis time and high tap density are key conditions for the commercialization of electrode materials. Carbon coated three-dimensional porous $LiFePO_4$ microspheres are synthesized by a supercritical and spray-dry combination method in a significantly short processing time (about 10 min). The three-dimensional (3D) porous morphology is composed of nanocrystallites tightly compacted to form three-dimensional electronic and ionic channels, which enhances their electrochemical properties. The obtained porous $LiFePO_4$ microspheres are intensively analyzed by XRD, SEM, TGA, and FT-IR techniques. The porous microspheres, which are 60 μm in size, show uniform morphology with the carbon coating. Moreover, at a 0.1 C rate the 3D porous microspheres of $LiFePO_4$ exhibit a high initial capacity with a high tap density (1.7 g cm^{-3}) and high active material content (~90% without carbon), which corresponds to 94% and 79% of the theoretical capacity at 0.1 and 1 C.

Introduction

Layered $LiCoO_2$ and spinel $LiMn_2O_4$ have been utilized as cathode materials for lithium secondary batteries. However, the cathodes have a disadvantage in thermal and electrochemical safety, which is due to oxygen release from lithium metal oxides under abuse conditions.[1] The oxygen release causes a rapid increase of the temperature in the battery which may lead to an explosion of the battery.

As a substitution for lithium metal oxides, $LiFePO_4$ has gained considerable attention as a cathode material because it is less expensive, more abundant, and environmentally benign. In addition, $LiFePO_4$ exhibits a high thermal stability and gives an extremely flat charge/discharge profile at ~3.4 V *versus* Li^+/Li. It also facilitates stable operation of the cell by providing a large over-voltage margin for oxidative electrolyte decomposition. Because the structural rearrangement due to lithium ion extraction/insertion in $LiFePO_4$ is small, the material can exhibit excellent cycling properties.[2,3]

However, $LiFePO_4$ has inherent poor electrical conductivity and slow Li ion diffusion. To overcome these intrinsic limitations of $LiFePO_4$, many researchers have reported that carbon-coating $LiFePO_4$ was effective in improving its electrochemical properties.[4–7] At the same time, highly crystalline small particles have been prepared by various methods to enhance the electrochemical properties of $LiFePO_4$.[8–12]

In an earlier study, we observed that the parameters of solid state synthesis processes, such as the ball milling time, firing temperature and duration, can considerably influence the properties of highly crystalline small particles of $LiFePO_4$.[13] A modified solid state synthesis was subsequently developed by incorporating additional steps to achieve a uniform carbon coating over the active particles, which could enhance the electrochemical performance.[14,15] Moreover, high porosity $LiFePO_4$ was optimized in a sol–gel process,[16] which enhances charge transport by increasing the amount of interface between the electrode and electrolyte. However, these synthesis processes are difficult to commercialize because of too many steps and long times. Teja's group produced $LiFePO_4$ nanoparticles prepared by sub- and supercritical water with a batch-type and continuous-type process that can synthesize in a relatively short processing time.[17,18] Also, Li *et al.* synthesized $LiFePO_4$ by a microwave-assisted synthesis method with a shortened processing time.[19]

The nanoparticles can contribute to the high rate capability by shortening the diffusion length of lithium ions and maximizing the interfacial contact between the nanoparticles and the surrounding electrolyte.[20] Nevertheless, nano-$LiFePO_4$ particles which increase the capacity decrease the tap density of the battery, which is an important factor to be considered in fabricating conventional batteries in industry. The nano-sized $LiFePO_4$ has a low tap density of less than 1.0 g cm^{-3}, but micro-sized $LiFePO_4$ can reach a tap density of 1.6 g cm^{-3}.[21–23]

[a] *Interdisciplinary School of Green Energy, Ulsan National Institute of Science and Technology (UNIST), 689-798 Ulsan, Korea. E-mail: jaekwang@unist.ac.kr*
[b] *Department of Applied Physics, Chalmers University of Technology, 412 96 Göteborg, Sweden*

† Electronic supplementary information (ESI) available. See DOI: 10.1039/c3ce42264j

The solid microspheres have long ion and electron transportation paths compared with nano-sized particles, and show poor electrochemical properties because the electrolytes cannot easily penetrate into the internal phase of the microspheres and conductive carbon can only coat the external surface of the solid microspheres. Therefore, the ideal architecture for $LiFePO_4$ with both a high tap density and high capacity should be a microsphere composed of nanocrystallites tightly compacted to form three-dimensional electronic and ionic channels.

In this study, three-dimensional (3D) porous $LiFePO_4$ microspheres are primarily synthesized by a supercritical and spray drying combination process. The use of a 3D porous microsphere electrode material offers an efficient method for increasing the interfacial area and decreasing the lithium ion diffusion distance, allowing for fast charge transport and an improved power capability with a high tap density. Supercritical synthesis is an improved process to prepare $LiFePO_4$ nanoparticles in a very short period of time and the spray method is useful to prepare three-dimensional microspheres with relatively fast aggregation of nanoparticles. Moreover, the 3D structure can offer more electrolyte transport paths for electron transfer and cation diffusion, which allows enhanced charge transport efficiency through the electrodes during the electrochemical reaction and leads to a good electrochemical performance.

Results and discussion

Fig. 1 is an SEM image of the porous $LiFePO_4$ microspheres, showing the uniform and well developed 3D microsphere morphology of the carbon coated $LiFePO_4$. All the powders show 3D porous spherical features. The typical size of the spheres is in the range of 25 μm to 60 μm, which perfectly replicates the morphology and size of $LiFePO_4$ (Fig. 1a). Fig. 1b is the black circled area in the inset of Fig. 1a. Close observation of the 3D-$LiFePO_4$ reveals that the mean diameter of the nano-sized particles is around 80 nm (Fig. 1b). Different particle morphologies correspond to the difference in particle interaction forces. Furthermore, the $LiFePO_4$ particles prepared from LiOH tend to grow larger in size because of the much lower melting point of LiOH, which allows the products to be crystallized and agglomerated into large particles. The spheres are enlarged after a thermal treatment in comparison with the spray-dried powders, indicating dilatation of the spheres during the decomposition of LiOH, $FeSO_4$ and *o*-H_3PO_4. The porous feature of the spheres is helpful for the penetration of the liquid electrolyte.

Fig. 2 shows the XRD spectrum of the Rietveld refinement for the 3D porous $LiFePO_4$ microspheres synthesized by the supercritical and spray combination method. The XRD pattern of the pure $LiFePO_4$ shows an absence of parasitic peaks, and all the diffraction peaks can be indexed to the orthorhombic olivine framework with the space group *Pnma*, being in agreement with high-crystalline single phase $LiFePO_4$ according to the JCPDS (no. 40-1499). The results of the Rietveld

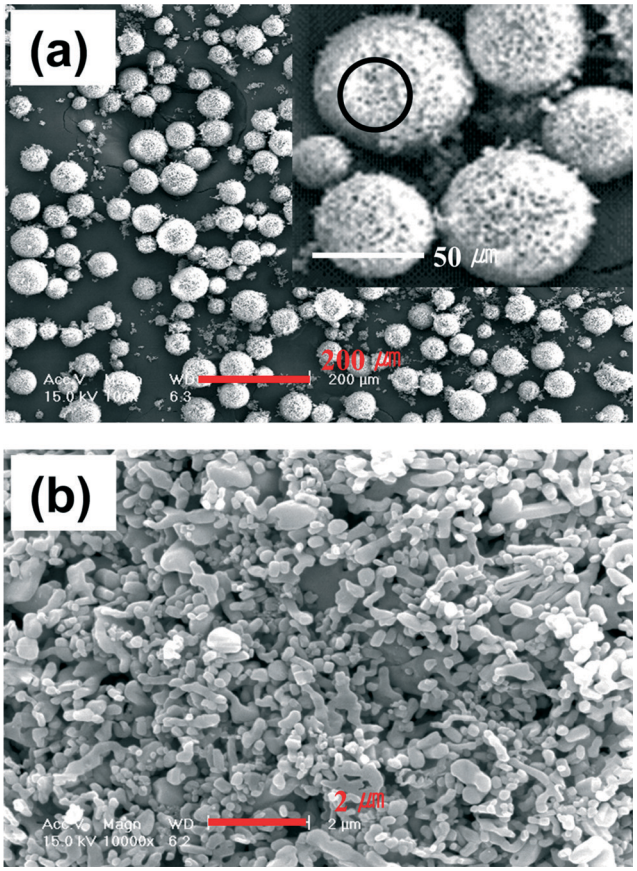

Fig. 1 SEM images of the carbon-coated 3D porous $LiFePO_4$ microspheres at two different magnifications. Q4

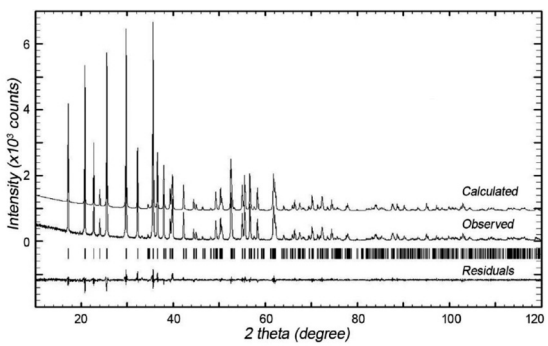

Space group: *Pnma*, R_p=8.03%, R_{wp}=10.7%, R_{exp}=7.57%, R_B=3.28%, S=1.4, χ^2=1.27

Cell parameters: a=10.3234Å, b=6.0056Å, c=4.6973Å, V=292.225Å^3

Fig. 2 X-ray diffraction pattern and Rietveld refined result of the carbon-coated 3D porous $LiFePO_4$ microspheres. The continuous line at the bottom shows the difference between the observed and calculated intensities.

refinement are summarized in Table 1. The lattice parameters of the $LiFePO_4$ microspheres are a = 10.323 Å, b = 6.005 Å, and c = 4.697 Å, corresponding to a volume of V = 292.225 Å.^{3} The grain size and the crystallite size (D) based on the (311) diffraction peak is calculated using Scherrer's equation:[13,24] $D = \kappa\lambda/\beta \cos\theta$, where k = 0.9, λ = 1.5406 Å, and β is the full width at half maximum length of a diffraction peak,

Table 1 Structural and cell parameters of the carbon-coated porous $LiFePO_4$ microspheres using Rietveld structure refinement

Atoms	Position	*x*	*y*	*z*	*B*
Li	4a	0	0	0	0.8
Fe	4c	0.2821(1)	0.25	0.9732(3)	1.0
P	4c	0.0959(2)	0.25	0.4198(4)	0.9
O1	4c	0.0955(5)	0.25	0.737(1)	0.8
O2	4c	0.4551(5)	0.25	0.2144(9)	0.8
O3	8d	0.1651(3)	0.0480(5)	0.2861(6)	0.8

respectively. The *D*(311) value is 21.5 nm resulting from Scherrer's equation.

The local structure of the 3D-$LiFePO_4$ is studied by FT-IR in the spectral range of 200–1400 cm^{-1}. The FT-IR is useful to detect an impurity. Fig. 3a shows the spectra of the 3D porous $LiFePO_4$ microspheres from the low wave number (300–600 cm^{-1}) to the high wave number region (600–1300 cm^{-1}). The lower number region involves bending modes of the active symmetric and asymmetric (υ_2–υ_4) P–O bond. The high wave number region (600–1300 cm^{-1}) involves stretching vibrations of the symmetric and asymmetric (υ_1–υ_3) modes of PO_4 groups. We do not find the Li_3PO_4 impurity of 424 cm^{-1} and $LiFeP_2O_7$ is also not detected on two bands at 769 and 1182 cm^{-1}, which are the symmetric stretching mode of P_2O_7 pyrophosphate groups and the vibration of the PO_3 groups, respectively.[25] The percentage value of the mass loss is taken from the TGA curve (Fig. 3b) and can represent an impurity of an amorphous phase. It can be seen from Fig. 3b that the weight below 200 °C drops sharply (from 100 to 99% is not sharply may be "slightly" is correct) from 100% at the starting temperature to about 99%, corresponding to the removal of moisture from the sample. After the removal of moisture, the curve is constant without weight loss to 800 °C, indicating non-impurity of amorphous.

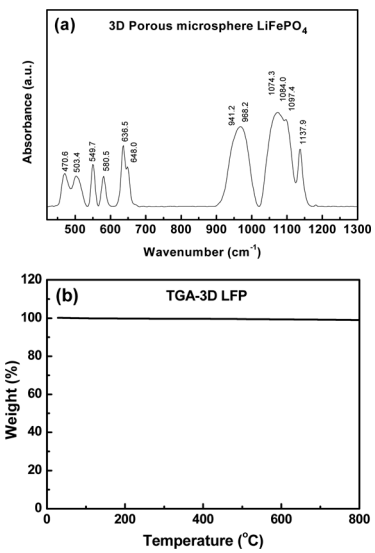

Fig. 3 (a) FT-IR spectra and (b) TGA curve of the carbon-coated 3D porous $LiFePO_4$ microsphere.

Detailed structural and morphological information is further characterized using TEM. In the TEM of the 3D porous $LiFePO_4$ microspheres, $LiFePO_4$ in the internal section is black, indicating that the $LiFePO_4$ nanoparticles are solid, which is in accordance with the SEM images (Fig. 4). The lattice fringe of $LiFePO_4$ and no lattice fringe of the carbon coating appear in the image and the selected area electron diffraction (SAED) pattern is shown in the inset of Fig. 4. As shown in the TEM, the 3D-$LiFePO_4$ is composed of numerous nanoparticles with an average diameter of 60 nm. The agglomerated $LiFePO_4$ nanoparticles can contribute to the decrease of the diffusion path of Li^+ ions and offer more active sites for electrochemical reactions. The wrapping of the carbon coating on the surface of $LiFePO_4$ can provide an ultrafast electron transfer and a capacious container for electrolyte penetration into internal phases.[20] Lithium is extracted on the (101) crystal surface as the phase boundary progresses in the direction of the *a*-axis. Li is constrained to move mainly parallel to the *b*-axis, and the (101) plane is active for Li ion extraction and insertion. Reducing the size of the particles in the *ac*-plane will have an impact on the electronic percolation within the electrode material. The indicated lattice fringes in Fig. 4 correspond to the (101) plane of olivine $LiFePO_4$ and the interplanar spacing of the *c*-axis is 4.8 Å, which is almost the same as the result of the Rietveld refinement. Also, the crystal size calculated by SAED and the high resolution image is 22.4 nm, which is similar to the XRD result.

The 3D porous $LiFePO_4$ microspheres, obtained with and without the carbon coating (3.3 wt.%) during the spray process, have been evaluated as cathode materials for their electrochemical performance in lithium cells at room temperature. The initial charge–discharge performances of the cells with pure 3D-$LiFePO_4$ cathodes are compared with those of the carbon-coated 3D-$LiFePO_4$ cathodes at a current density of 0.043 mA cm^{-2} (0.1 C-rate) in Fig. 5. The charge/discharge profile appears with the typical voltage plateau, attributed to the two phase reaction of the $(1 - x)FePO_4 + xLiFePO_4$ process. The difference between the charge and discharge

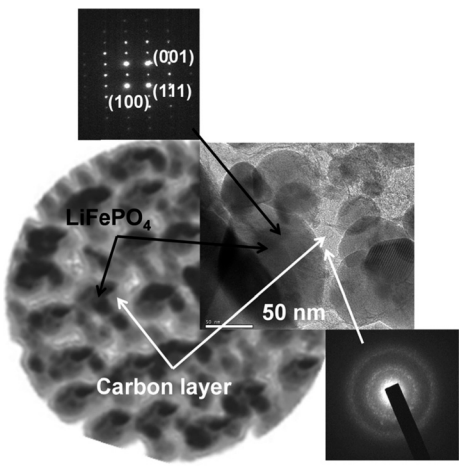

Fig. 4 TEM images of the carbon-coated 3D porous $LiFePO_4$ microspheres and the SAED patterns of $LiFePO_4$ and the carbon coating.

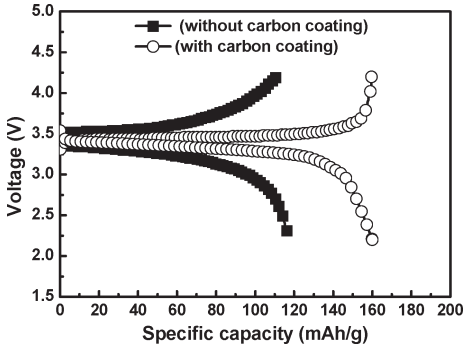

Fig. 5 Initial charge–discharge curves at a rate of 0.1 C in lithium cells with pure porous $LiFePO_4$ microspheres and carbon-coated porous $LiFePO_4$ microspheres (3.3 wt.% carbon) as cathodes.

voltages (ΔV) of the pure porous $LiFePO_4$ microspheres and the carbon-coated porous $LiFePO_4$ microspheres is minimal, 0.24 V and 0.19 V at 0.1 C respectively, indicating good kinetics of the redox reaction in the carbon coating due to the improved electrical conductivity. The carbon-coated porous $LiFePO_4$ microspheres exhibit a reversible capacity of 160 mAh g^{-1}, corresponding to a utilization efficiency of 94%, which confirms the high Coulombic efficiency (99%) of the redox process. However, before the carbon coating was applied, the width of the plateau was smaller with a 68% utilization efficiency. The curve of the carbon coated 3D-$LiFePO_4$ has a significant slope in the range of $0.7<X<1$ during the charge process and in the extended range of $0.6<X<1$ during the discharge process.

The short-term cycle performance (10 cycles each at different C-rates) of the Li/3D-$LiFePO_4$ cell is shown in Fig. 6. The capacity drops with an increase in the current density, indicating the capacity loss is restricted by lithium ion diffusion. At each current density, the porous $LiFePO_4$ microspheres deliver reversible discharge capacities of 153.4 mAh g^{-1} at 0.2 C, 145.4 mAh g^{-1} at 0.5 C and 133.7 mAh g^{-1} at 1 C-rate. The 3D porous $LiFePO_4$ microspheres show a good cycling property even at a high current density corresponding to 1 C with a high tap density of 1.7 g cm^{-3}. After a few initial cycles, the cells exhibit stable cycle properties at all the C-rates measured. It is also evident from this figure that the carbon coated porous $LiFePO_4$ microspheres have the capability of returning back to the original performance level when the C-rate is decreased. Thus, the performance of the cell at 0.1 C after subjecting it to 1 C is nearly the same as its initial property at 0.1 C, indicating that the electrode and formed solid electrolyte interface (SEI) layer are quite stable during cycling.

Fig. 7 shows the cycling performance and Coulombic efficiency of the 3D- $LiFePO_4$ microspheres at a rate of 0.1 C. The 3D-$LiFePO_4$ shows a high initial volumetric discharge capacity of 273 mAh cm^{-3} and also exhibits excellent cycleability with no noticeable decrease in performance over 50 cycles. The volumetric discharge capacity loss is less than 1% and the Coulombic efficiency remains close to 100%. Thus, the overall capacity fade of the microspheres, calculated on the basis of the initial and 50th cycle capacities, is ~0% per cycle. The results clearly demonstrate that the 3D porous $LiFePO_4$ microspheres are promising materials for cathodes of lithium batteries because of their high tap density, good capacity, excellent cycle stability, and high rate capability. These properties could be attributed to the agglomerated nanoparticles in the carbon-coated microspheres, providing a shorter diffusion distance for the Li^+ ions, while the carbon coating layer on the surface of $LiFePO_4$ could effectively enhance the electrical conductivity and hasten the transport of electrons.

Experimental

Degassed solutions of iron sulfate heptahydrate ($FeSO_4{\cdot}7H_2O$) in orthophosphoric acid (o-H_3PO_4) and lithium hydroxide (LiOH) were contacted with hot compressed water in a mixing tee of 33.5 MPa, 653 K, resulting in the precipitation of $LiFePO_4$ particles. All the chemicals were used as received from Aldrich (purity ≥ 98%). Since this reaction only leads to the precipitation of $LiFePO_4$, the precursor solution was adjusted to maintain the ratio of $FeSO_4{\cdot}7H_2O$: o-H_3PO_4 : LiOH at 1 : 1 : 2 in the experiments so that the mixture pH was ~7. The heterogeneous mixture of the particles and a sucrose solution was spray dried in a spray dryer at a rate of 15 ml min^{-1} at 473 K. The 3.3 wt% carbon-coated porous

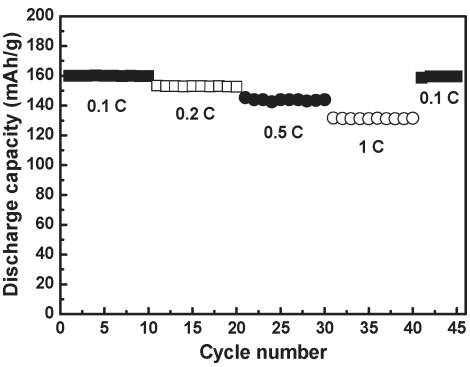

Fig. 6 Short-term cycling of the carbon-coated 3D porous $LiFePO_4$ microsphere cells at different C-rates (10 cycles at each C-rate, 25 °C, 2.2–4.2 V).

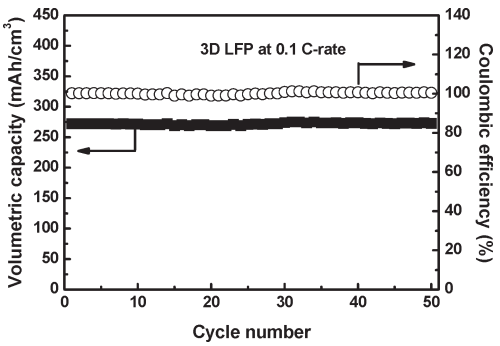

Fig. 7 Cycling performance, Coulombic efficiency and volumetric capacities of the 3D $LiFePO_4$ microsphere cell at 0.1 C between 2.2–4.2 V and at room temperature.

$LiFePO_4$ microspheres were obtained by carbonization of sucrose in a tube furnace at 973 K (Fig. S1, ESI†). The molar ratio of Li : Fe : P in the sample of $LiFePO_4$ was 1.1 : 0.9 : 1 (±0.02) and agreed with the theoretical ratio.

The chemical composition of the material was determined by inductively coupled plasma (ICP) analysis (Atomscan 25, Optima 4300DV) and the carbon content was determined by elemental analysis (CHNS-932, LECO). X-ray diffraction (XRD) was carried out with a D8 Advance, Bruker AXS apparatus equipped with a CuKα X-ray source (λ = 1.5406 Å) and FT-IR absorption spectra were recorded with a Fourier transform interferometer (VERTEX 80v, Bruker Optics). The data for the Rietveld structure refinement were obtained in the 2θ range of 15–120° with a 0.02° step interval and a 10 s step time. The sample was rotated (30 rpm) during the data collection to minimize any preferred orientation and statistical errors in the calculations. The crystal structure was refined in the space group *Pnma* using the program FullProf. TGA analysis was carried out in the temperature range of 30–800 °C and 10 °C min^{-1} on a thermobalance model SDT Q600, TA (USA) using Pt crucibles and under nitrogen.

The cathodes were prepared by mixing the active material powder, super-p carbon black (TIMCAL) and a PVdF binder in the ratio 90 : 5 : 5 by weight and the viscous slurry in *N*-methyl-2-pyrrolidinone (NMP, Aldrich) solvent was cast on aluminum foil and dried at 95 °C under vacuum for 6 h. The film was cut into circular discs with an area of 0.95 cm^2 and mass ~4.0 mg for use as the cathode. Two-electrode electrochemical coin cells were assembled with lithium metal as the anode material, a Celgard®2200 separator, 1 M $LiPF_6$ in EC : DMC (1 : 1 vol.%, Samsung Co.) electrolyte and $LiFePO_4$ as the cathode. Electrochemical performance tests were carried out using an automatic galvanostatic charge–discharge unit, WBCS3000 battery cycler, between 2.2 and 4.2 V at room temperature. The experiments were carried out at different current density rates from 0.1 to 1 C.

Conclusions

Three-dimensional porous $LiFePO_4$ microspheres have been synthesized with a uniform morphology and ~60 μm particle size by a supercritical and spray-drying combination method in 10 minutes. The morphology favors a shorter diffusion length for lithium ions, while the exterior conductive carbon coating provides connectivity for facile electron diffusion, resulting in a good electrochemical performance. The 3D porous $LiFePO_4$ microspheres display a high tap density of 1.7 g cm^{-3} and a high initial discharge capacity of 160 mAh g^{-1}, corresponding to a 94% theoretical capacity, and even at 1 C the reversible capacity is as high as 133.7 mAh g^{-1}. Also, a high volumetric capacity of 273 mAh cm^{-3} at a rate of 0.1 C is achieved, which may be successfully used on an industrial production scale.

Acknowledgements

The present work was supported by the Chalmers Area of Advance – Energy.

Notes and references

1 J. R. Dahn, E. W. Fuller, M. Obrovac and U. Sacken, *Solid State Ionics*, 1994, **69**, 265–270.
2 A. K. Padhi, K. S. Nanjundaswamy and J. B. Goodenough, *J. Electrochem. Soc.*, 1997, **144**, 1188–1194.
3 A. S. Andersson, B. Kalska, L. Haggstrom and J. O. Thomas, *Solid State Ionics*, 2000, **130**, 41–52.
4 Y. Hu, M. M. Doeff, R. Kostecki and R. J. Finones, *J. Electrochem. Soc.*, 2004, **151**, A1279–A1285.
5 D. Jugović and D. Uskoković, *J. Power Sources*, 2009, **190**, 538–544.
6 Y. Kadoma, J. M. Kim, K. Abiko, K. Ohtsuki, K. Ui and N. Kumagai, *Electrochim. Acta*, 2010, **55**, 1034–1041.
7 M. Konarova and I. Taniguchi, *J. Power Sources*, 2010, **195**, 3661–3667.
8 M. Gaberscek, R. Dominko and J. Jamnik, *Electrochem. Commun.*, 2007, **9**, 2778–2783.
9 G. Kobayashi, S. Nishimura, M. S. Park, R. Kanno, M. Yashima, T. Ida and A. Yamada, *Adv. Funct. Mater.*, 2009, **19**, 395–403.
10 M. Konarova and I. Taniguchi, *J. Power Sources*, 2009, **194**, 1029–1035.
11 A. Kuwahara, S. Suzuki and M. Miyayama, *J. Electroceram.*, 2010, **24**, 69–75.
12 J. W. Fergus, *J. Power Sources*, 2010, **195**, 939–954.
13 J. K. Kim, G. Cheruvally, J. W. Choi, J. U. Kim, J. H. Ahn, G. B. Cho, K. W. Kim and H. J. Ahn, *J. Power Sources*, 2007, **166**, 211–218.
14 J. K. Kim, J. W. Choi, G. Cheruvally, J. U. Kim, J. H. Ahn, G. B. Cho, K. W. Kim and H. J. Ahn, *Mater. Lett.*, 2007, **61**, 3822–3825.
15 J. K. Kim, G. Cheruvally, J. H. Ahn, G. C. Hwang and J. B. Choi, *J. Phys. Chem. Solids*, 2008, **69**, 2371–2377.
16 J. K. Kim, J. W. Choi, G. S. Chauhan, J. H. Ahn, G. C. Hwang, J. B. Choi and H. J. Ahn, *Electrochim. Acta*, 2008, **53**, 8258–8264.
17 J. Lee and A. S. Teja, *Mater. Lett.*, 2006, **60**, 2105–2109.
18 C. Xu, J. Lee and A. S. Teja, *J. Supercrit. Fluids*, 2008, **44**, 92–97.
19 D. Li, Y. Huang, N. Sharma, Z. Chen, D. Jia and Z. Guo, *Phys. Chem. Chem. Phys.*, 2012, **14**, 3634–3639.
20 J. Zhao, J. He, J. Zhou, Y. Guo, T. Wang, S. Wu, X. Ding, R. Huang and H. Xue, *J. Phys. Chem. C*, 2011, **115**, 2888–2894.
21 J. Qian, M. Zhou, Y. Cao, X. Ai and H. Yang, *J. Phys. Chem. C*, 2010, **114**, 3477–3482.
22 M. Wang, Y. Yang and Y. Zhang, *Nanoscale*, 2011, **3**, 4434–4439.
23 J. K. Kim, J. Scheers, Y. J. Choi, J. H. Ahn and G. C. Hwang, *RSC Adv.*, 2013, **3**, 20836–20842.
24 M. A. E. Sanchez, G. E. S. Brito, M. C. A. Fantini, G. F. Goya and J. R. Matos, *Solid State Ionics*, 2006, **177**, 497–500.
25 A. A. Salah, P. Jozwiak, K. Zaghib, J. Garbarczyk, F. Gendron, A. Mauger and C. M. Julien, *Spectrochim. Acta, Part A*, 2006, **65**, 1007–1013.